Multi-radar observations of an isolated substorm development in the early evening to midnight sector

Uspensky, M. (1,5), P. Eglitis (2,1), N. Partamies (1), G. Starkov (3), A.Fabirovsky (4), H. Opgenoorth (2,1), T. Pulkkinen (1), R. Pellinen (1)

(1) Finnish Meteorological Institute, P.O.Box 503, FIN 00101 Helsinki
(2) Institute of Space Physics, SE-755 91 Uppsala
(3) Polar Geophysical Institute, Fersman st.,14, 184200 Apatity, Murmansk region
(4) Murmansk State Technical University, Sportivnaya st.,13, 183010 Murmansk.
(5) On leave from Murmansk State Technical University, mikhail.uspensky@fmi.fi

INTRODUCTION

The objective of this report is to complete the multi-instrumental pre-substorm/substorm case study by Karlsson et al .(2000) using the SuperDARN data and related analysis.

During this event the Finland CUTLASS radar monitored so-called SEEL echoes (SEEL: Subvisual Equatorward Edge of the diffuse Luminosity belt) and the low-latitude edge of the quit-time auroral oval during a prolonged time (Uspensky et al., 1999). Here we pay more attention to the initiation and details of an isolated double auroral substorm as it was seen in auroral radar backscatter. In our analysis we use data from the Finland and Iceland CUTLASS radars as well as from the Iceland West SuperDARN radar. The radar collecting area covers more than 3000 km along auroral zone and ~5 hours of local time. The UHF EISCAT radar was also operated during that time with antenna pointing along B in the area of the Finland radar observations. WIND monitored solar wind at X~19, Z~5 and Y~31 Re, i.e. close to, but in the Y-direction slightly outside of the bow shock in front of the magnetosphere. GEOTAIL was in the magnetosheath at X~11, Z~2 and Y~1 Re, i.e. just outside the subsolar magnetopause. Supporting ground-based instruments were the IMAGE and the DMI Greenland magnetometers also the FMI Muonio digital all sky camera.

Figure 1 shows the geomagnetic conditions preceding the substorm as it was seen by the Greenland and IMAGE magnetometer networks. One can see that for ~15 hours at noon, afternoon, and evening the auroral zone was dominated a wide and weak eastward electrojet with current density of ~0.1 A/m. The auroral zone negative X-bay magnitude during the substorm (after ~1930 UT) was 200-300 nT.

Figure 2 exhibits the instrumental configuration. Stokkseyri, Pykkviber and Hankasalmi are the radar sites of the Iceland West, Iceland East CUTLASS and Finland CUTLASS HF SuperDARN radars. Small open circles along the radar beams run through 2.5 deg, where the dotted lines show the GG grid and the dash-dotted lines show the GM grid. The solid lines from top to bottom are the model poleward and equatorward edges of the auroral oval and the equatorward edge of the diffuse luminosity belt (Starkov, 1994) at 1800 UT and for AL=140 nT. In area of the equatorward edge of the diffuse luminosity belt there is a typical location of the Finland radar SEEL echoes. The site names in the RHS part of the picture are the IMAGE magnetometer sites.

Figure 3 illustrates the SEEL echoes, which here can be seen as a red-yellow (i.e. wide-spectrum) strip run along equatorward boundary of the diffuse luminosity belt (dashed line)

in the center panel. The dotted and dash-dotted lines are the Starkov model poleward and equatorward boundaries of the auroral oval. As can be deduced from the elevation angle data (bottom panel), before 15 UT the SEEL echoes are 1/2F-layer backscatter, after 15 UT they are 1/2E-layer backscatter. After 1800 UT inside of the auroral oval one can see the F-layer echoes, which at ~1852 UT manifests the substorm growth phase suddenly starting to move equatorward. The gray echoes in the center panel are the low-velocity echoes, which represent mainly ground scatter. The heavy magenta lines are the auroral arc lower edge, the heavy green lines are the same for the diffuse luminosity structure. The vertical dotted lines and the black bottom bars at the top and center panel of Figure 3 represent intervals when WIND started to observe negative IMF Bz magnitudes.

In Figure 4 one can see how the Iceland West SD radar spectral width reacts to the five reversals of the IMF Bz to their negative values. The 1st, 2nd and 3rd pulses with magnitudes of 2-4 nT initiated a short-term convection enhancements, which were clearly visible around-magnetic noon (here it is ~13 UT) and early afternoon. The 4th pulse, which was in 2-3 times stronger, turned to become a trigger for the substorm growth phase.

Figure 5 shows how the Iceland West SD radar monitors the HF backscatter at the four radiated frequencies. The start of the substorm growth phase is better visible at the higher frequencies of ~14.5 and ~16.2 MHz. This is marked as a start of the F-layer echo motion to equatorward and poleward at ~1845-1850 UT. Note, the radar frequency scanning gave here worse the time resolution. However, the start of the substorm growth phase, as detected by the Iceland CUTLASS East and Finland CUTLASS also the Iceland West SD radars, occured approximately at the same time, which within the measuring accuracy was 1845-1855 UT (for the Iceland East and Finland radars it was 1850-1855 UT). In the noon and afternoon the Saskatoon, Kapuskasing and Goose Bay HF radars detected the growth phase initiation as an enhancement of the convection at 1846-1848 UT (not shown here), i.e. a few minutes earlier only than in the Scandinavian sector.

As a summary, let us note the due to the quiet geophysical background we could well see the radar reaction to the WIND IMF Bz turning to negative values, e.g at about of 1557 UT (Figure 4). The effect was seen in the polar cap F-layer auroral echoes and also in low-latitude E-layer echoes by the two Iceland radars slightly after 1600 UT (Iceland East data are not shown). These echoes moved equatorward with velocities close to the auroral oval diurnal motion.

A rise of the Finland radar F-layer echoes at 18 UT (Figure 3) looks also like a consequence of a change of the solar wind parameters. The growth of the solar wind particle density and dynamic pressure started at ~1753 UT during a positive IMF Bz (see Karlsson et al., 2000, their Fig.2). The growth phase initiation can be seen in the whole HF radar data at 1846-1855 UT as a convection increase or a start of the F-layer echo increased equatorward motion after the new gradual negative IMF Bz turn at 1834-1842 UT (see WIND and GEOTAIL data, Karlsson et al., 2000). Note the ~3 min motion delay for echoes to overcross one radar range resolution cell. This is about 20-25 min earlier than the other ground-based instruments detect the growth phase development. Around midnight the F-layer blob-like core of the growth phase initiation was located in the vicinity of the poleward arc inside the quiet-time auroral oval. In contrast, earlier in the evening, the F-layer growth phase core originated and traveled into the oval from the polar cap (see Figures 4,5 and 6).

Figure 6 combines the substorm-time data collected by the Finland CUTLASS radar, which line-of-sight is approximately perpendicular to the L-shells (upper panel), by the Iceland CUTLASS radar located higher in latitude and ~ 2 hours earlier in the local time also

looking roughly perpendicular the L-shells (beam 0, middle panel) and the same Iceland radar looking approximately along the L-shells in area which is ~1.5 hour earlier in the local time than for the Finland radar (beam12, bottom panel). One can see that the image of the substorm is totally different even if one looks at the same area regarding the Starkov auroral boundaries (as earlier, the dotted, dash-dotted, and dashed lines). The conclusion is that the substorm epicenter and the surrounding area is even more filled by the field-aligned irregularities than is usually suggested and than it can be seen by any single radar.

A common feature of the top and middle panels is the narrow spectral width of the signals, which persists at a shorter distant, frontal part of the echo regions. We suggest that this is a consequence of a smaller altitude size of the echo area in its frontal part where the ray trajectories find their first orthogonality points. Another feature in the top panel is that during the breakup and recovery phase the E-layer echoes cover the area where a very weak sub-visual diffuse auroral luminosity was located. Indeed, the auroral radar backscatter was co-located with the diffuse luminosity structure at its equatiorward side, but it was avoided to be slightly poleward, i.e. inside of a moderate diffuse luminosity background between the luminosity structure (green line) and the auroral arc (magenta line). The cause of it is probably the ray's overrefraction. So, we can conclude that the weaker diffuse luminosity exists equatorward of the diffuse luminosity structure shown. Between 1930-2000 UT one can see a ~20-min burst of E-layer ground scatter, which is a product of changes of the E-layer electron densities and (probably) the layer local tilt between the first and second onsets (Karlsson et al., 2000).

A-14-minute enhancement of the SSE ionospheric electric field up to 70 and even more than 100 mV/m in the EISCAT antenna beam (see the open-circle strip in bottom panels of Fig.7 at 1940-1954 UT) was not supported by the HF-backscatter. It occurred in an area, which was obviously favorable to detect echoes from a decreased E-layer ionisation. However how one can see from Fig.7 the echoes were seen there only before and after the time. The comparison at Fig.7 was done taking data from the 5th beam of the Finland radar, which well covered the EISCAT observational area. Note, the drawn meridional size of the E-layer antenna beam trace in Figure 7 (shown by small open circles) is at least by a factor of ~20 more than the its real ionospheric trace. Due to the small size of the EISCAT collected area we use the magnetometer data to estimate the most probable meridional size of the region with an electric field enhancement. At the IMAGE X-magnitudes one can find a 20-30% spike which coincides with the EISCAT E-field enhancement of 200-300% (Figure 8). This SSE moving geomagnetic short-time enhancement can be well seen nearly at the same time in the latitudinal interval of ~7 deg between BJN and PEL. We suggest here that the meridional size of the E-field enhancement is more than 100 km. It is qualitatively supported by the long (~10 min) duration of the E-field enhancement.

Looking at RHS bottom SNR panel we find ~7-8 dB echoes which were seen before and after the E-field enhancement. However there are no echoes during that strong E-field growth. To understand the event let us suggest a rough current flow continuity in the surrounding area during the E-field burst. It means that the conductivity and E-layer electron density should be modified in a manner opposite to the E-field, i.e. decreased by a factor 2-3. The latter is in rough accordance with the EISCAT measurements (see Figure 9). Now we can make a link to the backscatter physics.

The backscatter power product can be found through the backscatter volume cross-section (σ_v)

$$\sigma_v = \text{const}^* \; N^2 \; <(\Delta N/N)^2>^{1/2} \; f(k, \psi, \theta), \qquad (1)$$

where N is mean electron density, $<(\Delta N/N)^2>^{1/2}$ is the mean electron density fluctuation amplitude (EDFA) and $f(k, \psi, \theta)$ is the spatial power spectrum of the backscatter irregularities, which is itself a function of the irregularity wave number (k), the aspect angle (ψ) and the flow angle (θ). To simplify the case let us neglect the k-dependence and the flow angle dependence (no strong changes) suggesting that the EDFA is proportional to E^{γ}, where E is an ambient electric field. Then

$$\sigma_v = \text{const}^* \; N^2 \; E^{\gamma} \; f(\psi). \qquad (2)$$

To assure the rough ionospheric current flow continuity we suggest that the product of the E-field and the electron density $E^*N \sim$ const. Other factor is the aspect angle. During the E-field burst and the electron density decrease the E-layer aspect angle becomes exactly orthogonal since there are too small ionospheric refraction changes for any ray trajectory. Note, the existence of the exact rectilinear orthogonality of the Finland radar ray trajectories in this area for the E-layer altitude. Thus, during the burst the observational conditions are better than before it. So, we write equation, which describes the 7 dB signal before the burst and, e.g. 0 dB signal during the burst

$$0.2^* N^2 * E^{\gamma} * f(\psi_1) = (N/3)^2 * (3^*E)^{\gamma} * f(\psi_2).$$

From here one can find the exponent for the EDFA reaction on the electric field

$$\gamma = \lg (1.8^* f(\psi_1)/f(\psi_2)) \; / \; \lg 3.$$

Since the ratio $f(\psi_1)/f(\psi_2)$ is not well known except that it is less than 1, let us do an upper limit estimate taking the ratio equals to 1. Then for SNRs of 7-8 dB the exponent takes values of $\gamma < 0.32$-0.53, i.e the EDFA reacts on the E-field rather slackly. Such the EDFA"saturation" could be due to a natural progressive wave energy losses during the course of some EDFA overgrowth.

Summary

1. The substorm growth phase initiation from late morning over Canada to evening and close to magnetic midnight over Scandinavia was nearly simultaneous with ~10 minutes delay after a pulse of the negative IMF Bz starts to activate the dayside reconnection. In evening and midnight the delay was a few minutes longer.

2. In a addition to Karlsson et al. (2000) who found that " solar wind pressure pulse (around 1845 UT) was the trigger agent …. causing the initial substorm expansion" at ~1900 UT, using the cited SuperDARN data we found that the negative IMF Bz turn that started at ~1937 UT during an increased solar wind pressure was the trigger agent to seed the convection enhancement and the related substorm expansion at 1946-1950 UT.

References

1. Uspensky, M., P. Eglitis, H. Opgenoorth, G. Starkov, T. Pulkkinen, R. Pellinen, 1999, Magnetospheric and solar wind signatures in HF radar data, Proceedings of the SuperDARN Annual meeting, Reykjavik, , 57.1-57.4.

2. Karlsson S.B.P., H.J. Opgenoorth, K. Kauristie, M. Syrjasuo, T. Pulkkinen, M. Lockwood, R. Nakamura, P. Eglitis, G. Reeves, S. Romanov, 2000, Solar wind control of magnetospheric energy content: Substorm quenching and multiple onsets, J.Geophys.Res., 105, 5335-5356.

T. 3

GWCMs ← ~ 3300 km, ~5 hours → IMAGE

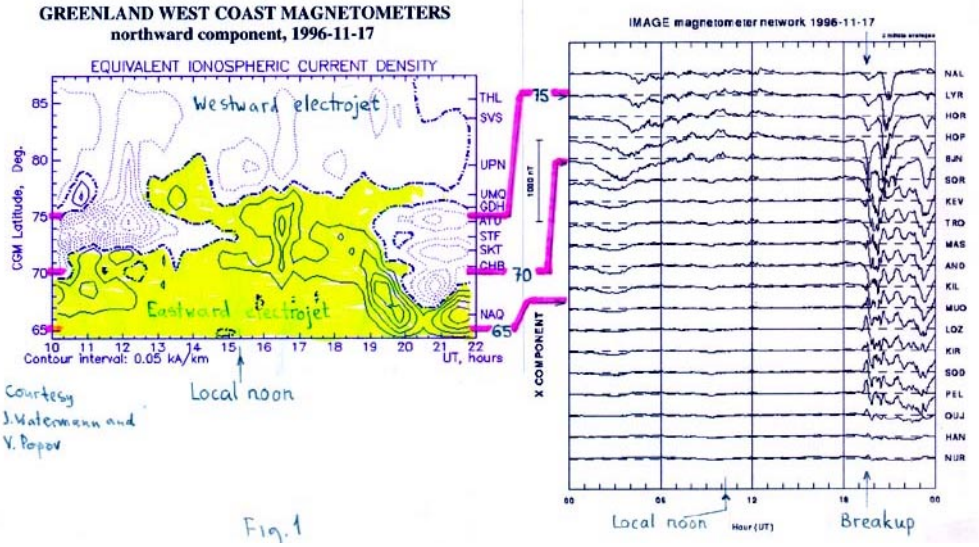

Courtesy
J. Watermann and
V. Popov

Fig. 1

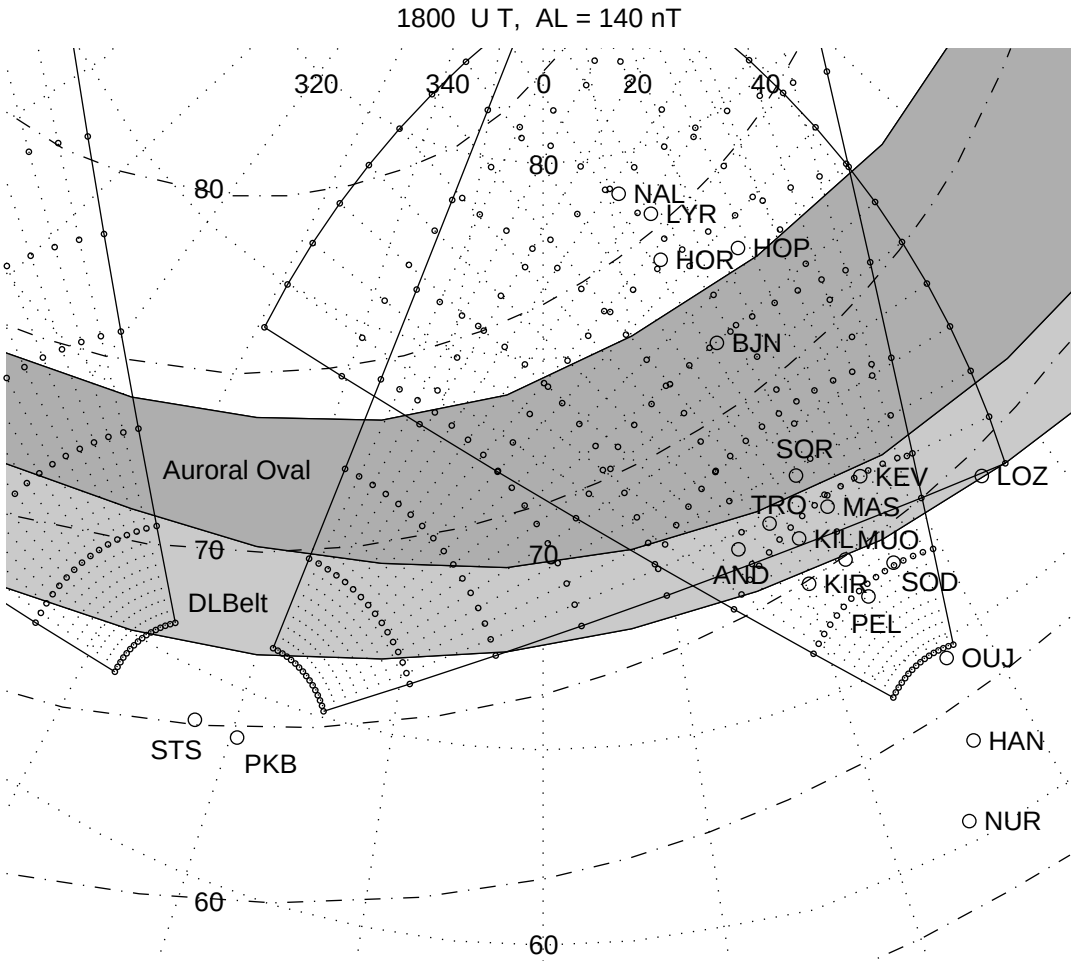
1800 U T, AL = 140 nT
320
340
0
20
40
80
80
NAL
LYR
HOR
HOP
BJN
SQR
KEV
LOZ
TRO
MAS
KIL
MUO
AND
KIR
SOD
PEL
OUJ
HAN
NUR
Auroral Oval
DLBelt
70
70
STS
PKB
60
60

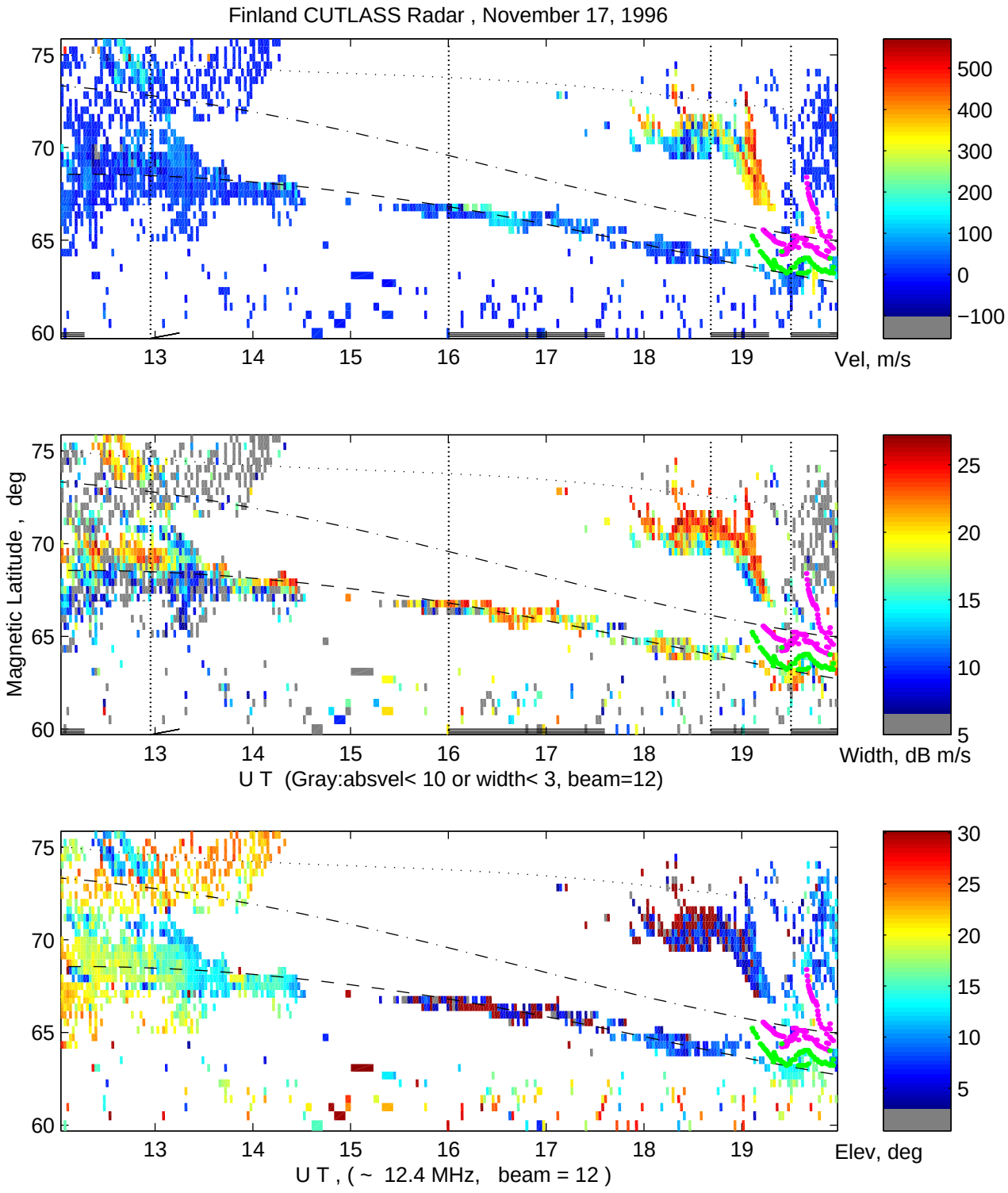
Finland CUTLASS Radar , November 17, 1996
75
70
65
60
13
14
15
16
17
18
19
500
400
300
200
100
0
−100
Vel, m/s
Magnetic Latitude , deg
25
20
15
10
5
Width, dB m/s
U T (Gray:absvel< 10 or width< 3, beam=12)
30
25
20
15
10
5
Elev, deg
U T , (~ 12.4 MHz, beam = 12)

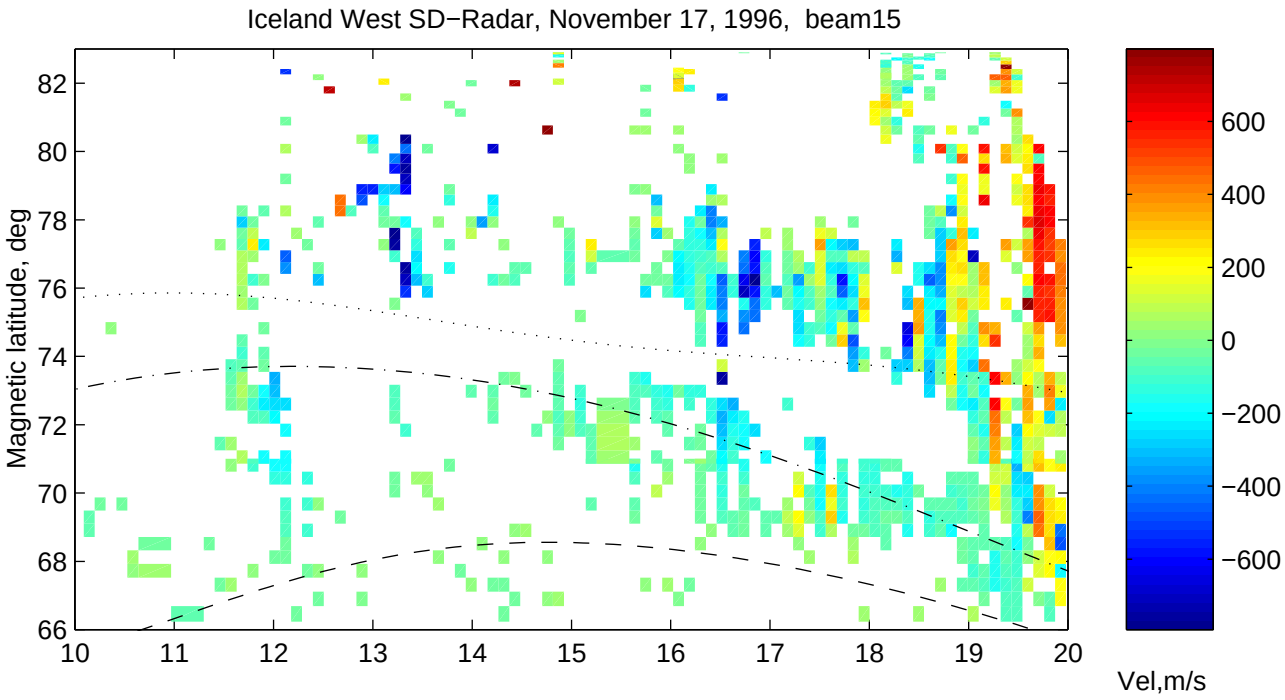
Iceland West SD−Radar, November 17, 1996, beam15
Magnetic latitude, deg
82
80
78
76
74
72
70
68
66
10
11
12
13
14
15
16
17
18
19
20
600
400
200
0
−200
−400
−600
Vel,m/s

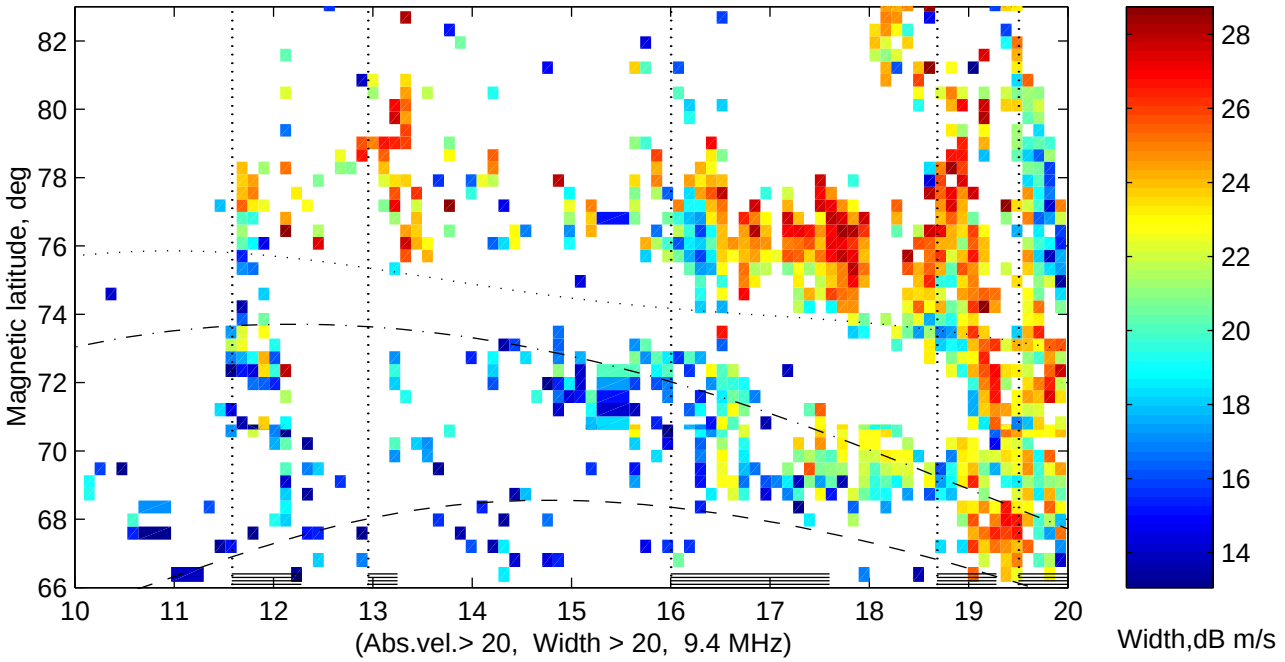
Magnetic latitude, deg
82
80
78
76
74
72
70
68
66
10
11
12
13
14
15
16
17
18
19
20
(Abs.vel.> 20, Width > 20, 9.4 MHz)
28
26
24
22
20
18
16
14
Width,dB m/s

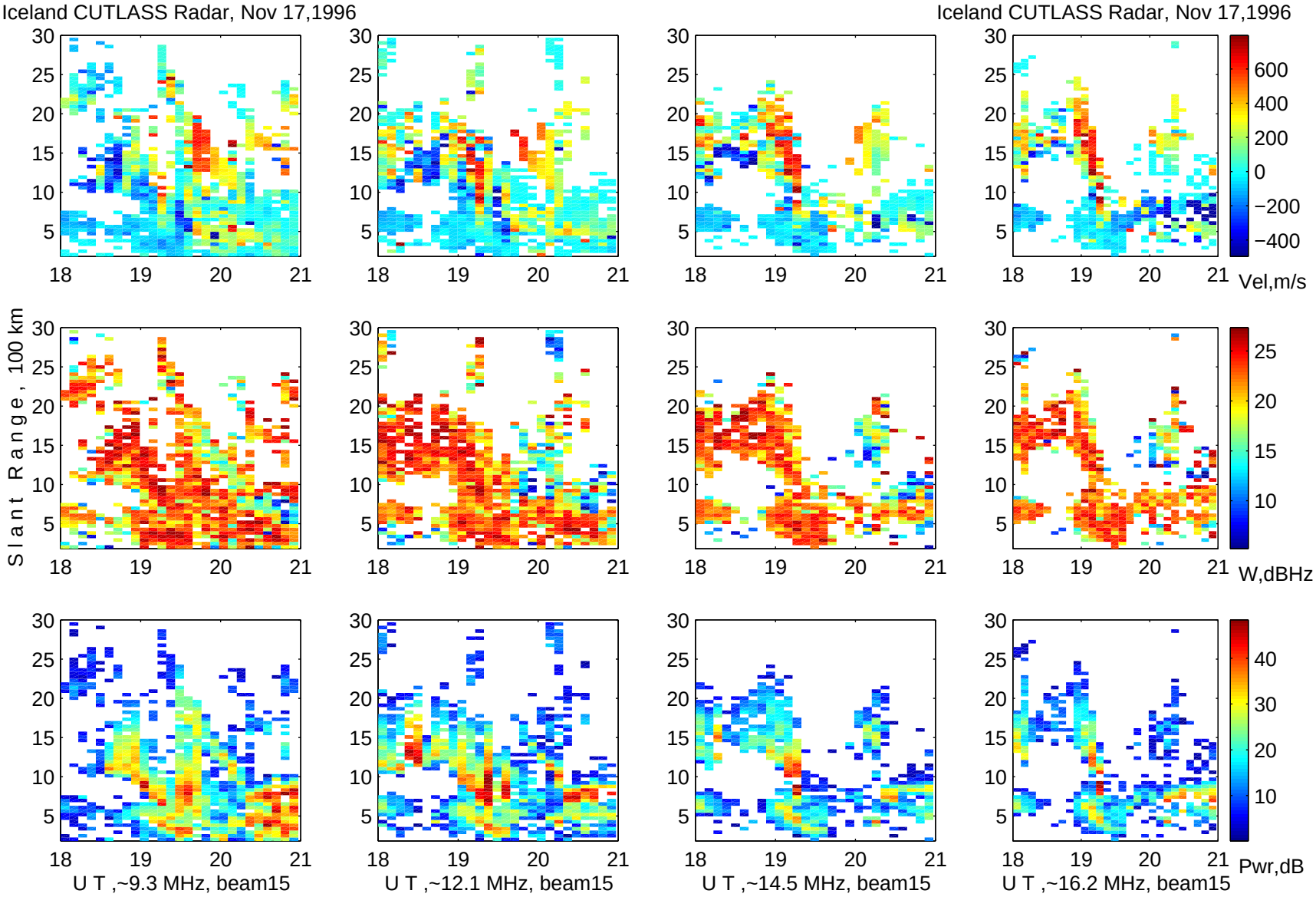
Iceland CUTLASS Radar, Nov 17,1996
Iceland CUTLASS Radar, Nov 17,1996
Slant Range, 100 km
Vel,m/s
W,dBHz
Pwr,dB
U T ,~9.3 MHz, beam15
U T ,~12.1 MHz, beam15
U T ,~14.5 MHz, beam15
U T ,~16.2 MHz, beam15

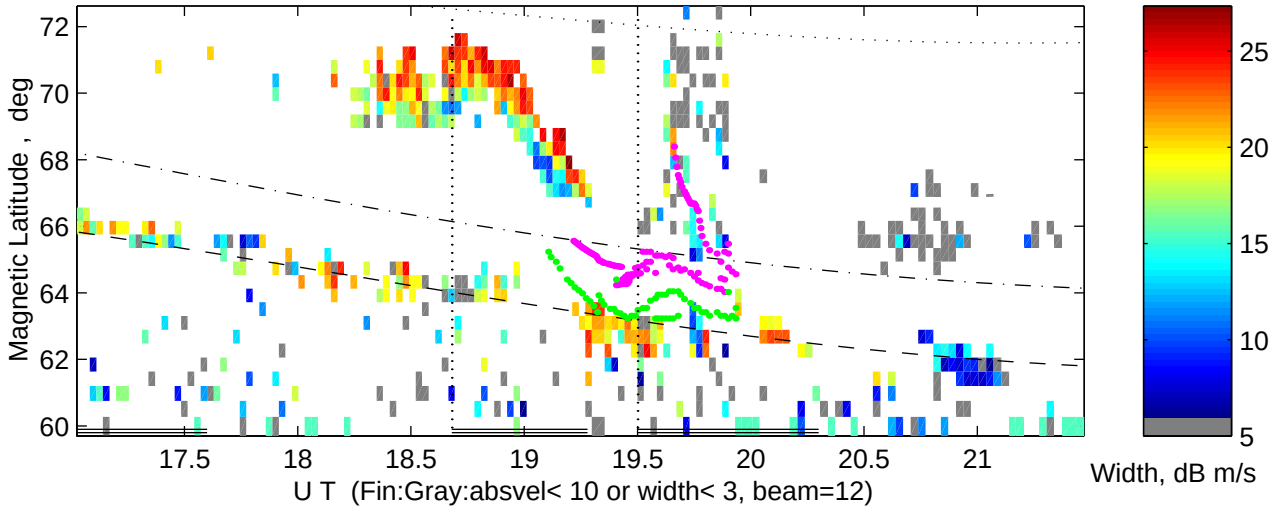
Magnetic Latitude , deg
72
70
68
66
64
62
60
17.5
18
18.5
19
19.5
20
20.5
21
U T (Fin:Gray:absvel< 10 or width< 3, beam=12)
25
20
15
10
5
Width, dB m/s

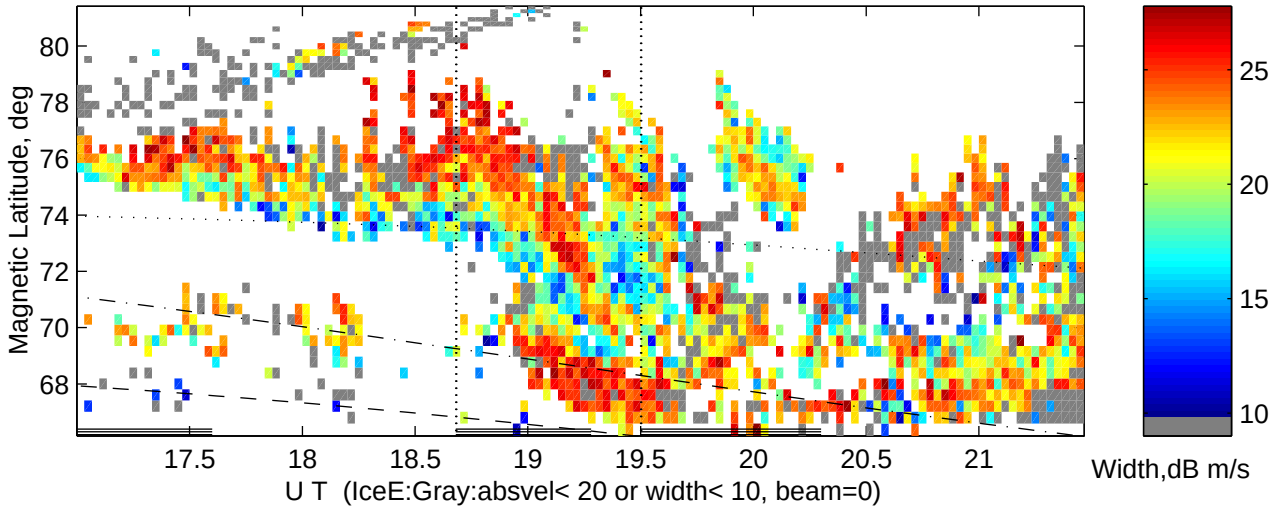
Magnetic Latitude, deg
80
78
76
74
72
70
68
17.5
18
18.5
19
19.5
20
20.5
21
U T (IceE:Gray:absvel< 20 or width< 10, beam=0)
25
20
15
10
Width,dB m/s

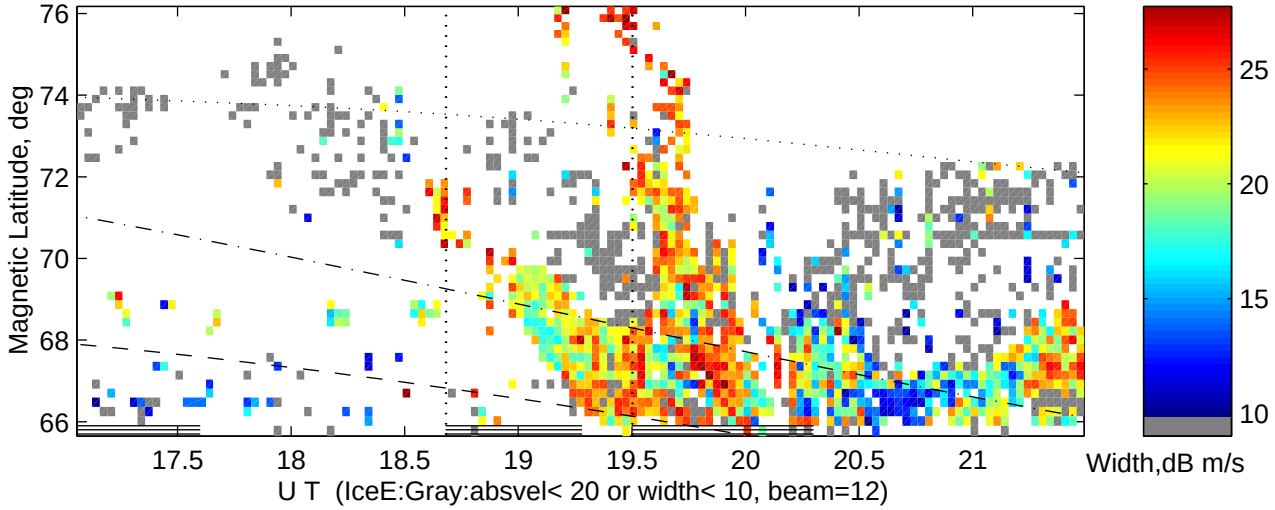
Magnetic Latitude, deg
76
74
72
70
68
66
17.5
18
18.5
19
19.5
20
20.5
21
U T (IceE:Gray:absvel< 20 or width< 10, beam=12)
25
20
15
10
Width,dB m/s

Finland CUTLASS Radar , November 17, 1996

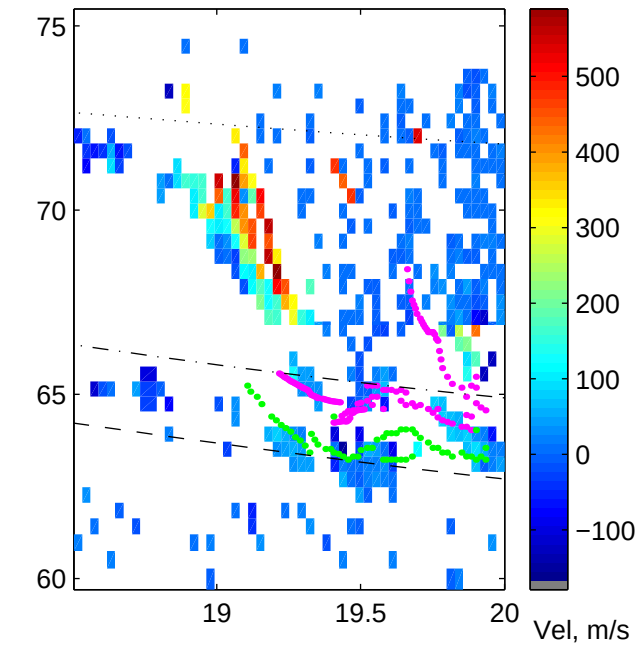

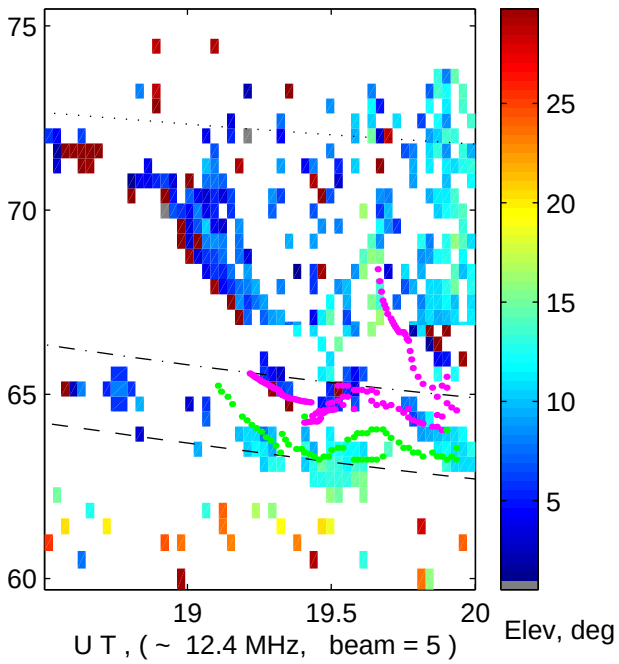

U T , (~ 12.4 MHz, beam = 5)

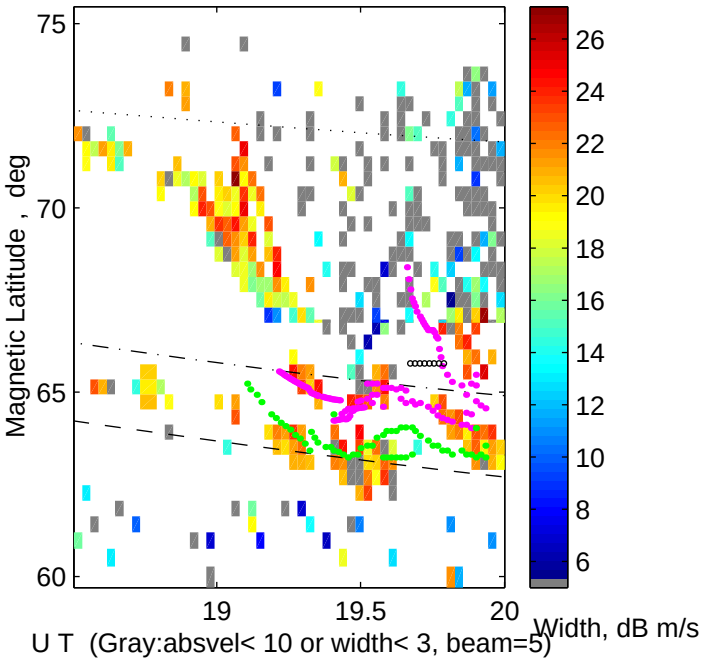

U T (Gray:absvel< 10 or width< 3, beam=5)

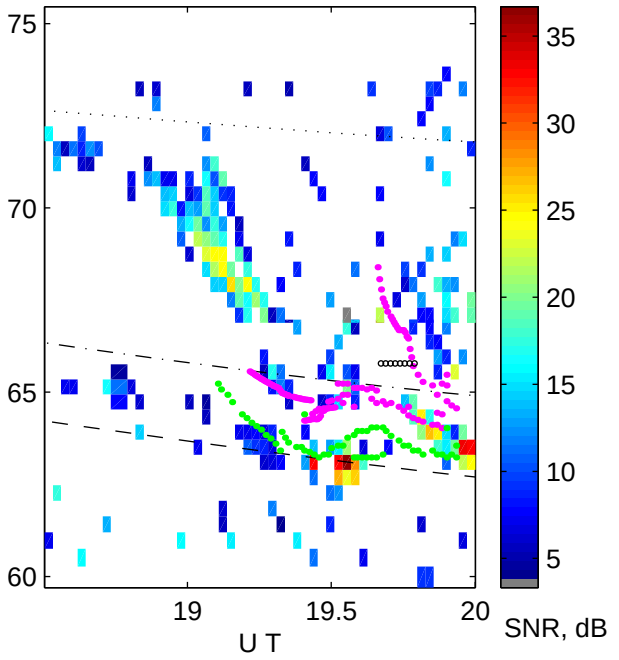

U T

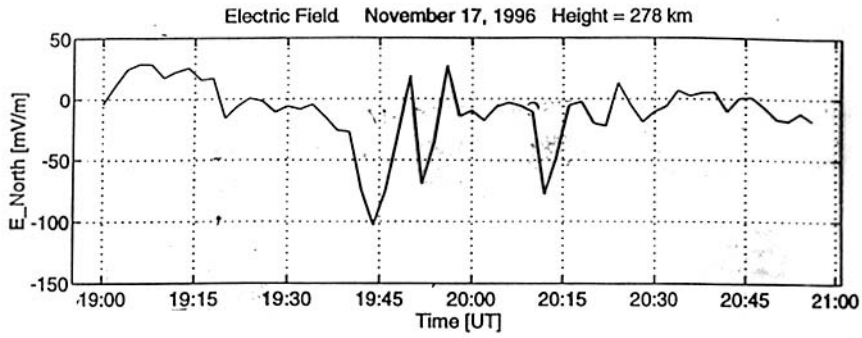
Electric Field November 17, 1996 Height = 278 km
E_North [mV/m]
50
0
-50
-100
-150
19:00
19:15
19:30
19:45
20:00
20:15
20:30
20:45
21:00
Time [UT]

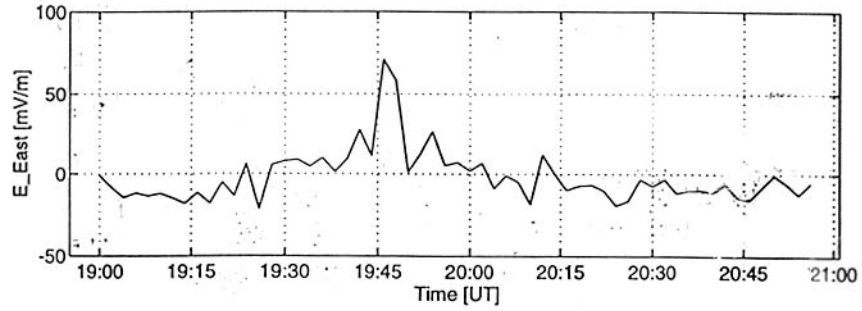
E_East [mV/m]
100
50
0
-50
19:00
19:15
19:30
19:45
20:00
20:15
20:30
20:45
21:00
Time [UT]

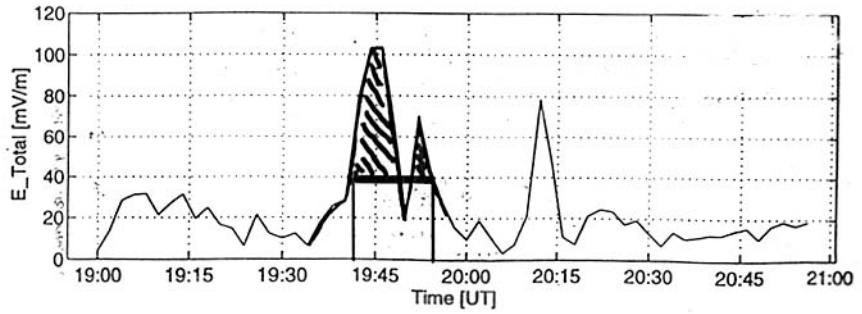
E_Total [mV/m]
120
100
80
60
40
20
0
19:00
19:15
19:30
19:45
20:00
20:15
20:30
20:45
21:00
Time [UT]

Fig. 8